Nuclear Instruments and Methods in Physics Research A 332 (1993) 142–148
North-Holland

NUCLEAR
INSTRUMENTS
& METHODS
IN PHYSICS
RESEARCH
Section A

Observation of Cherenkov rings using a low-pressure parallel-plate chamber and a solid cesium-iodide photocathode

N.S. Lockyer and J.E. Millan
Department of Physics, David Rittenhouse Laboratories, University of Pennsylvania, Philadelphia, PA 19104, USA

C. Lu and K.T. McDonald
Joseph Henry Laboratories, Princeton University, Princeton, NJ 08544, USA

A. Lopez
Department of Physics, University of Puerto Rico, Mayaguez, Puerto Rico, 00708

Received 13 October 1992 and in revised form 25 January 1993

We have observed Cherenkov rings from minimum-ionizing particles using a low-pressure, parallel-plate pad-chamber with a cesium-iodide solid photocathode. This detector is blind to minimum-ionizing particles, and sensitive to Cherenkov photons of wavelengths 170–210 nm. An average of 5 photoelectrons per Cherenkov ring were detected using a 2-cm-thick radiator of liquid C_6F_{14}. This paper reports on the chamber construction, photocathode preparation and testbeam results.

1. Introduction

Particle identification is essential for experiments that plan to study CP violation in the B-meson system. There are many B-meson decay modes that should exhibit CP violation, but the most precise information will come from the class of neutral CP-self-conjugate decay modes, such as $B \to J/\psi K^0_S$. The analysis of CP violation in such decays requires knowledge of whether a B or $\bar{B}$ produced the final decay products, and consequently the other B in the event must be "tagged" as a $\bar{B}$ or B. The charge of the K meson from B decays with the quark decay chain $b \to c \to s$ will tag with high efficiency the conjugation of the parent B meson. Cherenkov detectors provide a method of separating charged π's from K's and will therefore be important in the tagging process.

The Ring Imaging CHerenkov (RICH) detector [1] provides π and K identification over a greater momentum range than any other technique available. However, large RICH systems are difficult to build and operate at high rates and with high yields of photoelectrons.

RICH detectors using photomultiplier tubes perform well but are expensive to implement on a large scale, and insert a significant amount of material in the particles' path.

The largest and most ambitious existing RICH systems, such as those at SLD [2] and Delphi [3], use the photosensitive gas TMAE. For operation at atmospheric pressure a buffer gas is present, which typically is overly sensitive to minimumionizing particles and renders the detectors unstable at high gas gains. To achieve good detection efficiency the TMAE gas volume is large, leading to long collection times for the photoelectrons. The photoabsorption length, and hence the collection time can be shortened by raising the temperature of the TMAE gas [4,5]. However, the obvious operational and mechanical difficulties are such that at present no large system is proposed using this approach.

A variation on the TMAE gas detector employs a multistep-avalanche chamber where several stages of gain achieve high amplification while minimizing instabilities to photon feedback. These detectors still require heated TMAE gas to achieve a high absorption with a thin photosensitive layer [4–6].

In the present work we explore the use of low-pressure gas chambers with a solid cesium-iodide (CsI) photocathode. Such cathodes have been studied since the 1950s [7], and it is established under certain circumstances they deliver high quantum efficiency, but their performance is readily degraded by absorption of water vapor [8].

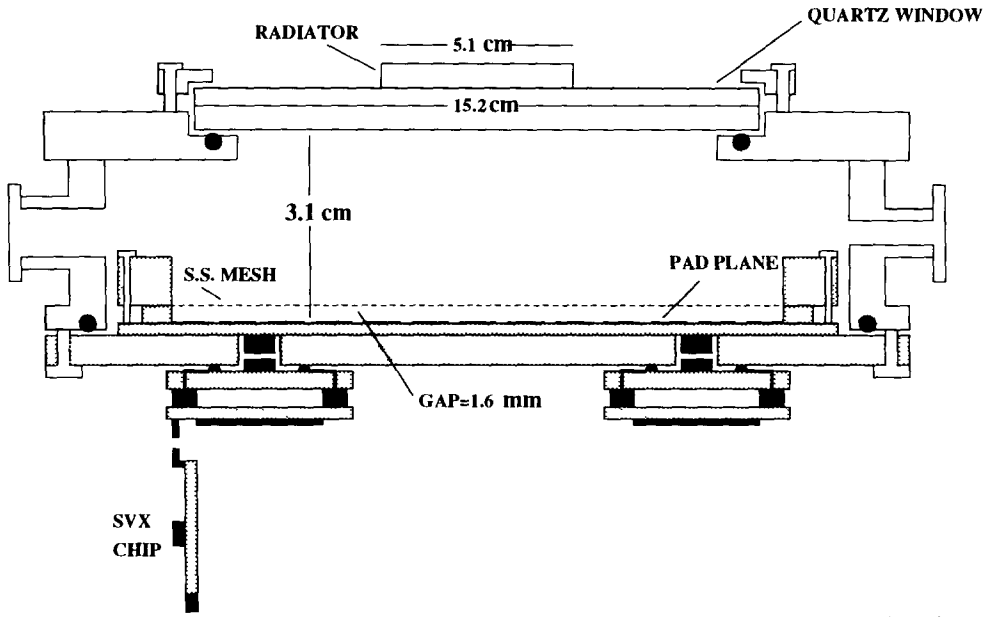

Fig. 1. Schematic view of the detector showing the radiator, low-pressure gas volume, semitransparent steel-mesh anode, pad-plane cathode, and configuration of printed-circuit boards on which the SVX readout chips are mounted.

In the last two years the work of the Anderson group at Fermilab [9–11], the Charpak group at CERN [12,14], the Ypsilantis group at Collège de France [13], and the Breskin group in Israel [15,16] indicates great promise for RICH detectors using high-quantum-efficiency CsI photocathodes. The fast time response of the solid photocathode [9,14] enables a RICH detector to be designed with a pad-chamber readout which will be appropriate for use at high-luminosity hadron colliders and B factories. Low-pressure operation renders the detector almost blind to minimumionizing particles, so they can be operated at very high gas gain. Furthermore, there is little loss of photoelectrons due to backscattering onto the cathode [17], and ion collec-

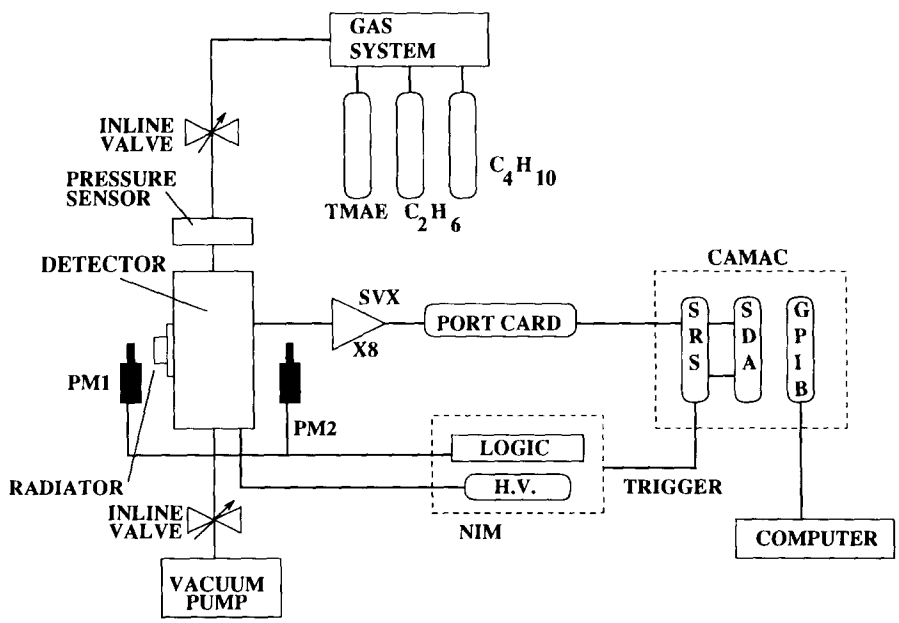

Fig. 2. Schematic of the experimental apparatus and the data-acquisition system.

tion times are minimized as the mean free path is long. CsI cathodes coupled to low-pressure chambers show good quantum efficiency for wavelengths up to ≈ 210 nm, so can be used with relatively inexpensive quartz windows. The resulting narrow sensitivity in wavelength (170–210 nm) minimizes chromatic dispersion as needed for good π/K separation.

We have built and tested a parallel-plate, low-pressure RICH detector with a CsI photocathode evaporated onto cathode pads. This paper presents details of the construction and performance of the detector when subjected to minimum-ionizing particles.

2. Detector description

2.1. Overview

The schematic layout of the RICH detector is shown in fig. 1. Particles enter from the top and traverse the liquid radiator. Cherenkov photons emitted in the radiator pass through the quartz window, through the gas at low-pressure enclosed in a stainless-steel vessel, through the steel-mesh anode plane, and photoeject electrons from the CsI photocathode on the surface of the cathode-pad plane. Each copper pad is instrumented with its own preamplifier channel of an SVX readout chip [18] which connects to a CAMAC-based data-acquisition system [19], sketched in fig. 2.

Cherenkov light is emitted by relativistic particles crossing the radiator of index n and thickness l at angle $\theta_C = \cos^{-1} 1/n$, and fills a circle of radius $r = l \tan \theta_C$ at the exit of the radiator. After the light crosses a gap of thickness L to the photodetector it occupies a ring of (inner) radius $R = L \tan \theta$ and thickness r, where $\sin \theta = n \sin \theta_C$ according to Snell's law. Thus we employ the method of "proximity focusing" i.e., no focusing at all, to allow the ring to spread out laterally. For good π/K separation the ratio r/R must be small.

In the present detector a Cherenkov ring has an outer radius $R + r = 6.3$ cm after a drift of 1.2 cm in the quartz windows and 3.1 cm in the chamber gas. This is somewhat smaller than optimal for use in high-energy experiments, but keeps the prototype suitably compact. The pad size is 8×8 mm^2 for a total of 332 pads over the 9-cm-radius active area.

2.2. Radiator

We use C_6F_{14} (index = 1.273 at 206 nm [3], item FC-72 of the Fluorinert Products Division of 3M Corporation, St. Paul, MN) as the radiator. The optical transmission over a 1-cm path was measured with a Perkin–Elmer $\lambda 3$ spectrophotometer, after purification with molecular sieve, to be 60% at 190 nm and rising to > 90% above 220 nm. We have since shown the optical transmission can be improved to > 84% at 190 nm by using Oxisorb (MG Industries, Valley Forge, PA) and that the molecular sieve is not needed, consistent with the experience of other groups [2,3].

The radiator was contained in a cylindrical spectrophotometer cell made from Suprasil quartz (Type 35, NSG Precision Cells, Farmingdale, NY). The liquid thickness is 2.0 cm, the inner diameter of the cell is 5.0 cm, and the walls are 0.1 cm thick. The cell has a Teflon plastic stopper and is mounted just outside the quartz window of the detector.

2.3. Chamber construction

Cherenkov light enters the chamber through a 15.2-cm-diameter, 1.1-cm-thick UV fused-silica window (Wilmad Glass Company, Buena, NJ) in the detector. The transmission is typically 90% for wavelengths greater than 170 nm. The vacuum seals between the window and chamber body, and between the chamber body and endplate are made with O-rings.

Gas amplification of photoelectrons occurs in a homogeneous electric field between the cathode-pad plane and the anode-mesh plane. The pad plane is connected to ground through the readout chips. The mesh plane is located 1.6 mm from the pad plane and is held at about +600 V.

The mesh plane is constructed from 80%-transparent stainless-steel cloth made of wire 27 μm in diameter with 270 μm spacing (Gerard Daniel and Co., New Rochelle, NY). The mesh-plane was stretched by a square frame and soldered onto a 1.6-mm-thick copper-clad G-10 ring with the aid of stainless-steel flux.

The pad plane is constructed as a two-layer G-10 printed-circuit (PC) board, 23.5 cm in diameter and 3.2 mm thick. The top layer contains the active pad region 9.0 cm in radius surrounded by a copper guard ring of 11.5-cm outer radius. There are 332 8×8 mm^2 pads with 1-mm gaps etched through the copper. Plated-through holes connect the pads to 125 μm-wide traces on the bottom layer with 125 μm minimum spacing between traces. The traces lead to four 2×50-pin connectors (1.27 mm × 1.27 mm spacing) surface mounted on the bottom layer of the pad plane. A solder mask is deposited on the traces to inhibit contact with ground. The pad plane is fastened to the aluminum endplate with screws at eight points on its circumference.

The endplate has four 6-cm-long by 1.3-cm-wide oval slots that allow the four surface-mount connectors on the pad plane to mate with corresponding connectors on four Interface boards. These boards are fastened to the endplate and potted with RTV-162 to complete the vacuum seal of the detector.

Once the chamber is assembled with a photocath-

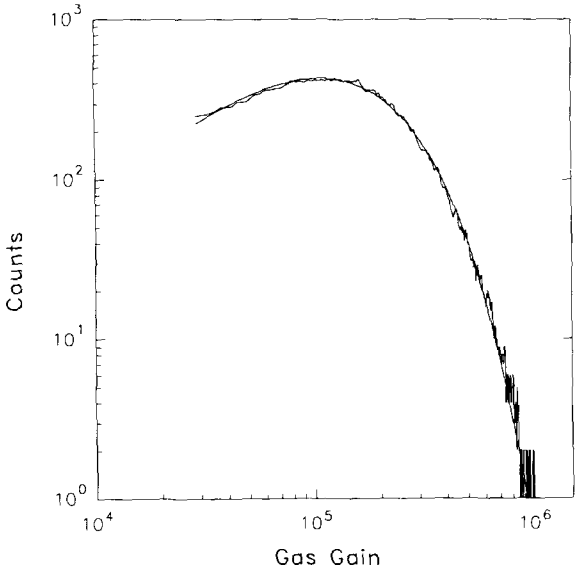

Fig. 3. The single-photoelectron gain spectrum fit to a Polya distribution: $P(g) \alpha (bg/\bar{g})^{b-1} e^{-bg/\bar{g}}$, where g is the observed gain, $\bar{g}$ is the average gas gain, and b is a measure of the fluctuation in gain [21]. The chamber was operated with 20 Torr of ethane and at 603 V. The fit was performed only for gain above 3×10^4 which determined that $\bar{g} = 2 \times 10^5$.

ode its performance as a single-photoelectron amplifier is verified using a pulsed hydrogen-discharge lamp (model TNLD14-01, Hamamatsu Co., Bridgewater, NJ) and a preamp (model 142PC, EG&G Ortec, Oak Ridge, TN) connected to a single pad, or group of pads. A typical single-electron spectrum obtained with ethane gas at 20 Torr is shown in fig. 3.

2.4. Readout system

The front-end of the readout system is based on the SVX data-acquisition chip, designed in VLSI technology at Lawrence Berkeley Lab [18]. A set of eight SVX chips mounted on the chamber amplifies the signals from all 332 pads and sends them to a CAMAC digitizing module [19].

To connect the SVX input lines to the pads in the chamber and to connect the SVX I/O pads to the external data-acquisition system, three PC boards were designed which we called the Interface, Protection-Circuit and SVX-Carrier boards. The Interface board brings the signals from inside the vacuum vessel out to a connector. The Protection-Circuit board plugs into this connector and protects the input of the SVX chip from high-voltage sparking in the chamber. The SVX-Carrier board contains the SVX chip and connectors that allow communication with CAMAC.

Several Interface board designs were tested to achieve a good vacuum seal without introducing significant leakage currents into the SVX inputs. While two-component, 5-min epoxy provided a good vacuum seal around the connector, it was slightly conductive and consequently the width of the SVX pedestals increased. This problem was alleviated by removing the epoxy and substituting Glyptol insulation paint. A solder mask over the traces on the Interface board insulates the signal lines from the aluminum endplate. A thin plastic cover with a slot in the center was glued on top of the surface-mount connectors on the Interface board, to provide a smooth surface for the O-ring seal between the board and the endplate.

PC-board technology cannot easily provide signal lines matched to the 50-μm spacing of the input pads of the SVX chip. We chose to bond only 42 of the 128 available SVX channels per chip. Promex Co. (Santa Clara, CA) mounted the chips on the SVX-Carrier board and the aluminum bonds performed well. A right-angle connector mates the SVX-Carrier board to the connectors located on the Protection-Circuit board. The signals are brought to the data-acquisition system with flat 50-conductor, 100 Ω cables.

An overview of the data-acquisition system is shown in fig. 2. The system is based on SRS and SDA CAMAC modules designed at Lawrence Berkeley Laboratory [19] and built for us at U. Oklahoma. These modules provide clock pulses for the SVX chips as well as digitization for the signals.

3. Cesium-iodide photocathode

3.1. Preparation

The photocathode consists of an evaporated layer of CsI on the copper-pad plane. We follow a procedure similar to that of ref. [11].

Heat is applied to the evaporator bell-jar with an infrared lamp while pumping down to a few $\times 10^{-7}$ Torr with a turbomolecular pump. (Oil-diffusion pumps are to be avoided.) The heating accelerates removal of water vapor. The tungsten boat is then heated to remove residues that may be present after previous evaporations. The evaporator is briefly opened to air and the scintillation-grade CsI crystal is placed on the evaporator boat. Roughly 0.2 μm of CsI is then evaporated, without the substrate (pad plane) installed in the evaporator to ensure the crystal is completely free of finger grease or other surface impurities.

The pad-plane substrate is cleaned with water, an abrasive material and ethyl alcohol. The evaporator is opened again to air and the substrate is mounted 30 cm above the boat. A 1.2-μm-thick layer of CsI is vacuum-evaporated onto the cathode-pad plane at a rate of approximately 30 Å/s.

Immediately after the evaporation, the bell-jar is filled with nitrogen gas to atmospheric pressure. This

step reduces the exposure of the photocathode to water vapor. The pad plane is removed from the bell-jar and installed into the detector vacuum vessel, a process that takes about 10 min and during which time nitrogen gas is continually flowed over the photocathode. The quantum efficiency is reduced by a factor of $\frac{1}{3}-\frac{1}{2}$ due to absorption of water vapor during this 10-min period, according to the experience of refs. [8,15].

3.2. Improvement of quantum efficiency by heating

We have measured the quantum efficiency of photocathodes produced as above relative to TMAE gas using a technique described by Hoeneisen et al. [9]. In this an additional mesh electrode is place in the chamber to form a low-field collection region for photoelectrons from TMAE gas. By suitable arrangement of voltages on the electrodes the chamber can then be operated with either a solid CsI photocathode, or a with a layer of photosensitive TMAE gas. The chamber is exposed to a hydrogen-discharge lamp and the ratio of count rates is observed for the two modes of operation. The results obtained with 300-mTorr TMAE gas must be corrected for 40% absorption in a 1.5-cm-thick field-free gap prior to the 1.42-cm thick collection gap, based on an average absorption coefficient measured by Anderson [20]. The dependence on wavelength of the quantum efficiency of CsI [11] and TMAE gas [22] is, by coincidence, very similar. Comparing to measurements of the absolute quantum efficiency of TMAE [22] we infer that the quantum efficiency of the CsI cathode is 13% at 190 nm, after the cathode has been subjected to the heating described below.

Following the procedure of ref. [11], after installation of the photocathode we began pumping on the chamber while heating the copper-pad plane to about 30°C. We applied the heat with an infrared lamp located 20 cm above the chamber endplate. Metal pins were inserted into the surface-mount connectors on the endplate to provide good thermal contact to the copper pads inside the detector. The temperature was measured with a thermocouple adhered to the pad plane. We also flowed nitrogen gas through the chamber to aid in removing surface contaminants.

During heating the rate of single photoelectrons induced by a hydrogen lamp was monitored as a measure of the quantum efficiency. The quantum efficiency improved by about a factor of two in about three hours during this treatment, but did not increase further with prolonged heating.

Applying heat to the chamber did not initially improve the quantum efficiency, rather it decreased by about a factor of two. It was realized that adhesives inside the chamber were outgassing rapidly during the heating process and were adhering to the photocathode. There were several possible sources of contami-

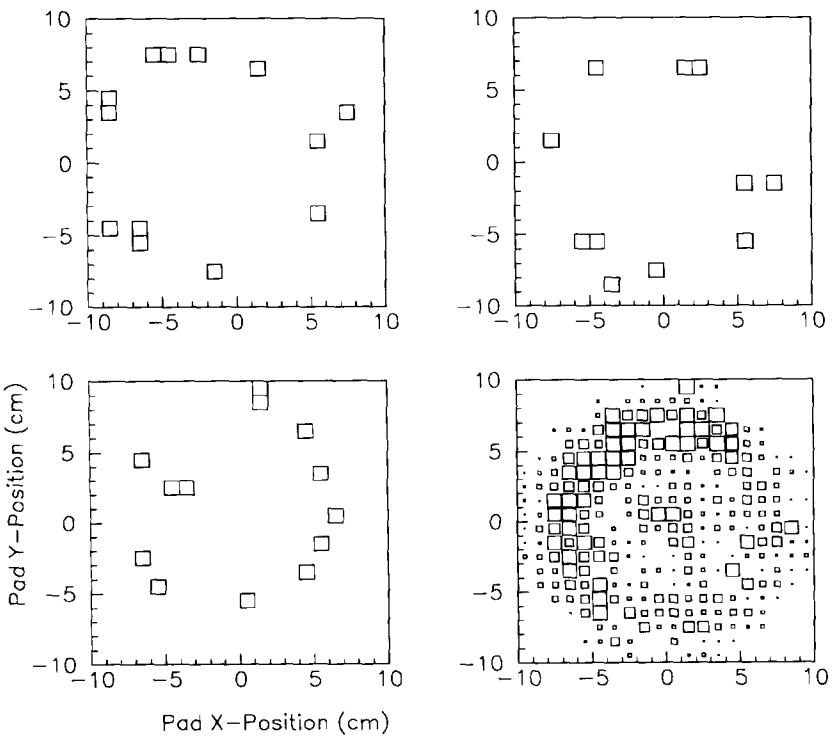

Fig. 4. Three plots are single-particle events displaying obvious rings. The fourth plot shows a sum of events from a short run.

nants in the chamber. We were using Kapton tape on the endplate to provide electrical isolation for the signals as well as on the G-10 mesh support ring. In addition, we had originally used Kapton heating tape with an adhesive backing to heat the pads prior to using the infrared lamp. We had also used 5-min epoxy to secure the wire mesh to the G-10 ring. Removing the adhesives and epoxy provided dramatic improvement in the quantum efficiency. Unfortunately, the final detector configuration still contains the adhesive from the thermocouple and a small quantity of single-component RTV-162 sealant. Clearly, future versions of the detector design should give great care to eliminating any substance that can outgas.

3.3. The effect of chamber gas on quantum efficiency

The gas in the chamber provides amplification of the photoelectron signal via Townsend avalanches. It also has a marked effect on the quantum efficiency. Low-pressure operation of the chamber with a CsI photocathode and ethane gas results in quantum efficiencies ($\approx 7\%$) for wavelengths around 190 nm almost an order of magnitude larger than vacuum operation ($\approx 1\%$) [7,11]. But if the gas pressure is increased to one atmosphere the quantum efficiency is reduced, presumably by large-angle scattering of photoelectrons back onto the cathode [17].

4. Testbeam studies

After completing the various laboratory tests of the detector described above we studied the performance of the detector in two testbeams, the M-Test beamline at Fermilab, and behind the C3 beamline dump at Brookhaven Lab. Although we had moderate success at Fermilab, the results presented in this paper are from data taken at Brookhaven.

Three single-particle events (with a larger than average number of hits) are shown in fig. 4 with struck pads indicated as squares. Each photoelectron typically excites one pad, and the ring is easily identified. The chamber gas was ethane at 20 Torr, and the chamber was operated at ambient temperature.

Shown in the lower-right of fig. 4 is the sum of hits over a short run. When adjacent pads were struck they were counted as only a single hit. The area of each bin reflects the summed number of hits. The general outline of the rings are seen to be enhanced, although there is smearing due to the transverse size of the radiator. The nonuniform density of hits around the ring is possibly due to uneven gain across the surface of the pad plane which resulted from a warping of the anode support ring during heating. Note that roughly 10% of the rings have a hit in their center, which

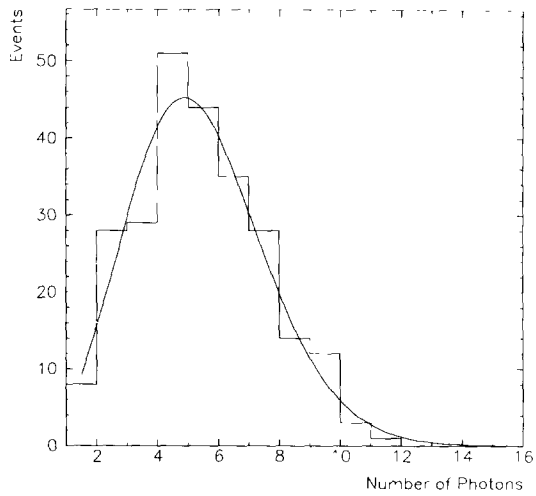

Fig. 5. The spectrum of the number of detected photoelectrons per event from minimum-ionizing particles, fit to a Poisson distribution of mean 4.9.

corresponds to the probability that a minimum-ionizing particle is detected.

The multiplicity distribution of hits per ring for this run is shown in fig. 5, for which the mean is $N = 4.9$ photoelectrons. We compare this with the expectation of $N = N_0 l \sin^2\theta_C = 0.77 N_0$ with $dN_0/d\lambda = 2\pi\alpha/\lambda^2 \times$ detection efficiency, $l = 2$ cm as the radiator length, and $\theta_C = 38°$ as the Cherenkov angle corresponding to index $n = 1.273$. The various efficiency factors are displayed as a function of wavelength in fig. 6. The transmission through the quartz windows is based on data from the vendor, corrected for reflection of the polarized Cherenkov light at the C_6F_{14}/quartz and

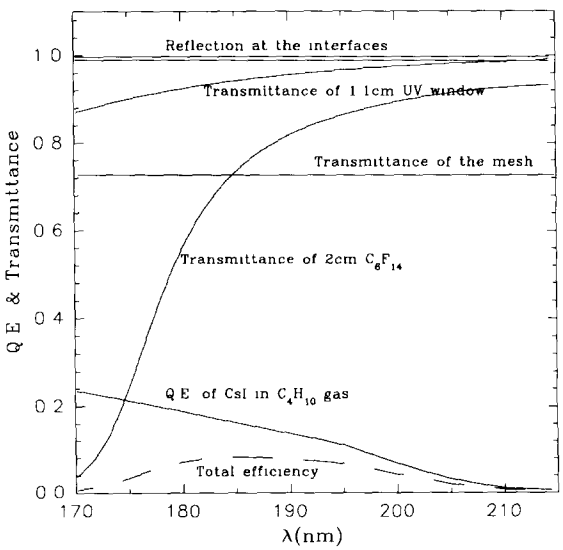

Fig. 6. Efficiencies as a function of wavelength that enter the calculation of the detector-quality parameter N_0.

quartz/vacuum interfaces; the cutoff is slightly below 170 nm. Because the Cherenkov angle is near the Brewster angle the reflection losses are very small. The transmission factor of the mesh anode is 0.73, which includes a factor of 0.9 for the effect of the angle of incidence (51°) of the Cherenkov photons. The transmission of the radiator is based on measurements with a spectrophotometer by us down to 190-nm wavelength, and extrapolated to the cutoff near 170 nm using data reported in ref. [3]. Note that the average path length for Cherenkov light produced over a 2-cm path is (1 cm)/cos θ_C. If the quantum efficiency of the photocathode with ethane gas followed the wavelength dependence reported by Anderson et al. [11] for isobutane gas (23% at $\lambda = 190$ nm) then we should have achieved $N_0 = 26$, and $N = 20$ photoelectrons per ring on average. The observed results are consistent with a quantum efficiency of only 0.26 that of ref. [11], i.e., about 7% at 190 nm.

This value is lower than our measurement of 13% for the quantum efficiency at 190 nm reported in section 3.2. Some 12 hours elapsed between the two measurements, during which time the photocathode was not heated and was transported from U. Pennsylvania to Brookhaven Lab. The quantum efficiency may well have deteriorated during this interval.

5. Conclusions

These results indicate that a RICH detector using a solid CsI photocathode coupled to a low-pressure, parallel-plate avalanche chamber is an excellent device for particle identification in future high-rate B factories, either hadron colliders or e^+e^- colliders. From the experience of ref. [11] we infer that the number of photoelectrons can be increased by a factor of four over our value of 4.9 by using better photocathode-preparation procedures. Purification of the liquid radiator with Oxisorb, as routinely used by SLD [2] and Delphi [3] will provide a further improvement of about 20%. The use of liquid C_8F_{18} may improve the photoelectron yield by 20–30% as its transmission cutoff lies below 180 nm. Such increases in quantum efficiency would permit the use of a shorter radiator and drift space, and operation at atmospheric pressure, both of which are desirable for compact, large-area RICH detectors.

Acknowledgements

We thank Bruce Hoeneisen of Universidad San Francisco de Quito and David Anderson, Sharon Austin and Simon Kwan of the Particle Detector Group at Fermilab for many useful discussions. George Kalbfleisch of U. Oklahoma rendered great assistance in the preparation of the SVX readout system. We thank Linda Stutte and Jonathan Streets of Fermilab and Alan Carroll and David Dayton of Brookhaven for beamline support. Craig Woody and Joe Fischer provided insight and assistance in the handling of TMAE and C_6F_{14} at Brookhaven. Finally, we thank three very good undergraduate students, Steve Peil, Toby Kessler, and Berthilla Weiss. This work was supported in part by the US Department of Energy grants DE-FG02-91ER40671 and DE-FG02-91ER40680 and by the Texas National Research Laboratory Commission grant RGFY9235.

References

[1] J. Séguinot and T. Ypsilantis, Nucl. Instr. and Meth. 142 (1977) 377.
[2] D.W.G.S. Leith, Nucl. Instr. and Meth. A265 (1988)120.
[3] R. Arnold et al., Nucl. Instr. and Meth. A270 (1988) 255, 289.
[4] A. Breskin et al., IEEE Trans. Nucl. Sci. NS-35 (1988) 404.
[5] V. Vasileiadis et al., Nucl. Instr. and Meth. A289 (1990) 618.
[6] G.B. Coutrakon, B. Biggs and S Dhawan, IEEE Trans. Nucl. Sci. NS-33 (1986) 205.
[7] A.H. Sommer, Photoemissive Materials (Wiley, New York, 1968).
[8] L. Heroux, W.J. McMahon and H.E. Hinteregger, Appl. Opt. 5 (1966) 1338.
[9] B. Hoeneisen, D.F. Anderson and S. Kwan, Nucl. Instr. and Meth. A302 (1991) 447.
[10] S. Kwan and D.F. Anderson, Nucl. Instr. and Meth. A309 (1991) 190.
[11] D.F. Anderson et al., Nucl. Instr. and Meth. A323 (1992) 626.
[12] V. Peskov et al., Nucl. Instr. and Meth. A269 (1988) 149.
[13] J. Séguinot et al., Nucl. Instr. and Meth. A297 (1991) 133.
[14] G. Charpak et al., Nucl. Instr. and Meth. A307 (1991) 63.
[15] V. Dangendorf et al., Nucl. Instr. and Meth. A289 (1990) 322.
[16] V. Dangendorf et al., Nucl. Instr. and Meth. A308 (1991) 519.
[17] D.F. Anderson et al., Nucl. Instr. and Meth. 217 (1983) 217.
[18] S. Kleinfelder et al., IEEE Trans. Nucl. Sci. 35 (1988) 171.
[19] F.A. Kirsten and C. Haber, IEEE Trans. Nucl. Sci. NS-37 (1990) 288.
[20] D.F. Anderson, IEEE Trans. Nucl. Sci 28 (1981) 842
[21] J. Byrne, Proc. R. Soc. Edin. A66 (1962) 33.
[22] R.A. Holroyd et al., Nucl. Instr. and Meth. A261 (1987) 440.